

Coherent diffractive photoproduction of ρ^0 mesons on gold nuclei at RHIC

STAR Collaboration

Abstract

The STAR Collaboration reports on the photoproduction of $\pi^+\pi^-$ pairs in gold-gold collisions at a center of mass energy of 200 GeV/nucleon. These pairs are produced when a nearly-real photon emitted by one ion scatters from the other ion. We fit the $\pi^+\pi^-$ mass spectrum to a combination of ρ^0 and ω resonances and a direct $\pi^+\pi^-$ continuum; the ratio of ρ^0 to direct $\pi^+\pi^-$ is consistent with previous measurements. The ω cross-section is comparable with that expected from the measured $\gamma p \rightarrow \omega p$ cross section, a classical Glauber calculation and the $\omega \rightarrow \pi^+\pi^-$ branching ratio.

The ρ^0 differential cross section $d\sigma/dt$ clearly exhibits a diffraction pattern, compatible with scattering from a gold nucleus, with 2 minima visible.

Keywords: Rho photo-production, diffraction, hadronic form factor

PACS: 25.75.Dw, 25.20.Lj, 13.60.-r

1. Introduction

Relativistic heavy ions are accompanied by high fluxes of nearly-real photons, due to their large electric charge and the strongly Lorentz contracted electric fields. These photons have virtuality ($\langle Q^2 \rangle \sim 2 \times 10^{-3} \text{GeV}^2$). In relativistic heavy ion collisions, these fields can produce photonuclear interactions. When they collide and interact hadronically, the strong interactions obscure these electromagnetic interactions. However, when they physically miss each other, the photonuclear interactions can be visible; these are referred to as Ultra-Peripheral Collisions (UPCs). The photon flux is well described within the Weizsäcker-Williams formalism [1, 2].

For photoproduction of ρ mesons at RHIC, the rapidity range $|y| < 0.7$ corresponds to photon-nucleon center of mass energies from 9 to 18 GeV, depending on the rapidity and final state transverse momentum. In this region, the ρ^0 photo-production cross section increases slowly with energy; the $\gamma p \rightarrow \rho p$ cross section is well described by the soft-Pomeron model [3].

A more detailed model considers the photon as a combination of Fock states: a bare photon with virtual $q\bar{q}$ pairs, plus higher virtual states. It was successful at describing many of the Deep Inelastic Scattering (DIS) measurements performed at HERA [6] and is also applicable in the UPC environment.

Many models have been proposed to describe the ρ photoproduction cross section in ultra-peripheral heavy ion collisions. The first calculation used HERA data on $\gamma p \rightarrow \rho p$ as input to a classical Glauber calculation to predict the cross section with heavy ions [7]; it successfully predicted the ρ photoproduction cross section at RHIC energies from 62 GeV/nucleon [8] to 130 [9] and 200 GeV/nucleon [10], and up to 2.76 TeV/nucleon at the LHC [11]. A later calculation treated the $q\bar{q}$ pair as a dipole in a quantum Glauber calculation, which found a cross section about 50% higher, in tension with the data [12]. Recently, a modification of the quantum Glauber calculation has been proposed; in this model nuclear shadowing reduces the calculated ρ cross section to match the data [13]. Other calculations include nuclear saturation mechanisms, including the colored glass condensate [14, 15]. Two-photon production of $\pi^+\pi^-$ pairs also occurs, but the cross-section is much smaller than for photonuclear interactions [16].

Because of the high photon flux these UPC events have a high probability to be accompanied by additional photon exchanges that excite one or both of the ions, into a Giant Dipole Resonances (GDR) or higher excitation. The GDRs typically decay by emitting a single neutron, while higher resonances usually decay by emitting two or more neutrons [17]. These neutrons have low momentum with respect to their parent ion, so largely retain the beam rapidity. For heavy nuclei, the total cross section for multi-photon interactions nearly factorizes [18], with the combined cross section given by an integral over impact parameter space:

$$\sigma(A_1 A_2 \rightarrow A_1^* A_2^* \rho) = \int d^2b P_{0\text{Had}}(b) P_1(A^*) P_2(A^*) P(\rho), \quad (1)$$

where $P_{0\text{Had}}(b)$, $P_1(A^*)$, $P_2(A^*)$ and $P(\rho)$ are the respective probabilities for not having a hadronic interaction, exciting the two ions and producing a ρ . Each photon-mediated reaction occurs via independent photon exchange, so all four probabilities are tied together only through a common impact parameter [19]. The photonuclear cross-sections are based on parameterized data [33]. The individual photon-mediated subreactions have a strong impact parameter dependence, so the combined probability is highest for impact parameters $b > \approx 2R_A$, where R_A is the nuclear radius. A unitarization process is employed to account for the possibility of multiple photons contributed to excite a single nucleus.

This letter reports on the measurement of exclusive ρ and ω meson and direct $\pi^+\pi^-$ photo-production in UPCs between gold ions using the Solenoidal Tracker At RHIC (STAR) detector at a center of mass energy of 200 GeV/nucleon. The current data sample is about 100 times larger than in previous measurements [10] at this energy. The improved statistics allow for much higher precision studies, leading to two main new results. First, the high-statistics $\pi\pi$ invariant mass distribution cannot be fit with just ρ and direct $\pi\pi$ components; an additional contribution from photoproduction of ω , with $\omega \rightarrow \pi^+\pi^-$ is required for an acceptable fit. The second is the observation of a detailed diffraction pattern, clearly showing the first and second minima, with a possible third. This

diffraction pattern can be used to determine the distribution of the hadronic matter in gold nuclei.

2. Experimental Setup and Analysis

This analysis uses an integrated luminosity of $1074 \pm 107(\mu b)^{-1}$ of data collected during 2010 (RHIC run 10). Five STAR components were used for triggering and event reconstruction in the analysis: the Time Projection Chamber (TPC), Time of Flight system (TOF), Beam Beam Counters (BBCs) and East and West Zero Degree Calorimeters (ZDCs).

The STAR TPC [20] efficiently detects charged tracks with pseudo-rapidities $|\eta| < 1.4$, using 45 layers of pad rows in a 2 m long cylinder. In the 0.5 T solenoidal magnetic field, the momentum resolution is $\Delta p/p = 0.005 + 0.004p$ with p in GeV/c [20]. The TPC can also identify charged particles by their specific ionization energy loss (dE/dx) in the TPC. The dE/dx resolution is 8% for a track that crosses 40 pad rows. This gives good pion/kaon/proton separation up to their respective rest masses. The TPC is surrounded by a time of flight system (TOF), covering pseudo-rapidity up to $|\eta| < 1$ [21]. For this analysis, the TOF system was used to reject tracks that are out of time with the beam crossing.

The other detector components were used solely for triggering. At higher rapidities, charged particles are detected using the two BBCs, one on each side of the nominal interaction point. Each is formed with 18 scintillator tiles arranged around the beam pipe, covering a pseudo-rapidity window of $2 < |\eta| < 5$ [21]. The ZDCs are small hadron calorimeters installed downstream of the collision region to detect neutrons at beam rapidity [22].

The trigger [?] selected 38 million events with small multiplicity in the central detector, along with one or more neutrons in each ZDC, along the lines described in [10]. It requires low activity in the TOF detector (at least two and no more than six hits), no charged particles detected in the BBC detectors and finally, showers in both ZDC detectors corresponding to at least the equivalent of one neutron with beam momentum or up to four beam momentum neutrons. The threshold on each ZDC calorimeter was set at 50 ADC channels (the centroid of the one neutron peak sits at 198 channels) making them fully efficient.

The analysis selected events containing a pair of oppositely charged tracks (like-sign pairs were used as a background measure) that were consistent with originating from a single vertex, located within 50 cm longitudinally of the center of the interaction region. The tracks were required to have at least 14 hits in the TPC (out of a possible 45), and have dE/dx values within 3σ of the expected dE/dx for a pion. Both tracks in each pair were required to have a valid hit in the TOF system; this cut rejected events from other beam crossings. It also limited the track acceptance largely to the region $|\eta| < 1.0$. The 384,000 events with a $\pi^+\pi^-$ pair mass in the range $0.25 < M_{\pi\pi} < 1.5$ GeV were saved for further evaluation.

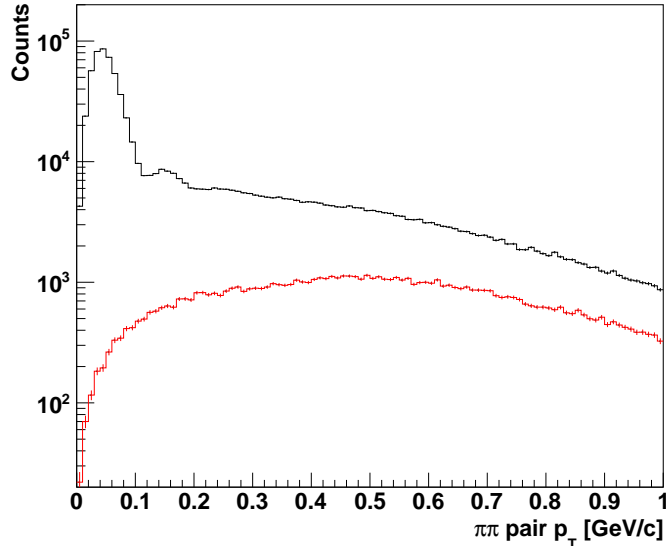


Figure 1: The black histogram shows the pion pair transverse momentum. The peak below 100 MeV/c is from the decay of coherently produced $\pi^+\pi^-$ pairs. The red histogram shows the pair momentum for same-sign pion pairs. Both histograms show pairs that come from vertices with only two tracks.

The largest backgrounds for this analysis were low-multiplicity hadronic interactions (peripheral ion-ion collisions), with some of their charged particles out of the TPC acceptance. Other backgrounds come from other UPC reactions or from cosmic-rays accompanied by in-time mutual Coulomb excitation. Pure electromagnetic production of e^+e^- pairs contribute less than 4% to the ρ peak [9]. The decay $\omega \rightarrow \pi^+\pi^-\pi^0$ produces a $\pi^+\pi^-$ pair below the ρ^0 peak, but with a larger p_T than for coherent ρ^0 photoproduction; it contributes a few percent (2.7% in a previous analysis [10]) to the measured incoherent $\pi^+\pi^-$ pairs. We neglect these minor backgrounds here; they are well within the overall systematic errors.

The hadronic backgrounds may be estimated from the like-sign pion pairs. Figure 1 compares the transverse momentum (p_T) of the $\pi^+\pi^-$ pair (black histogram) with the corresponding distribution for like-sign pairs (red histogram) in recorded vertices with only two tracks. The signal distribution has a prominent peak for $p_T < 100$ MeV/c. This peak is due to coherent photoproduction of pion pairs from the gold nucleus. In this region, the signal to noise ratio is very high; at larger p_T , the backgrounds are a larger fraction of the signal.

The reconstructed events are corrected for acceptance and detection efficiency using a detailed simulation of the STAR detector. A mix of ρ mesons and non-resonant $\pi\pi$ events are generated using the STARLight Monte Carlo [7] which reproduces the kinematics of the event, including the mass and rapidity

distributions. These events are sent through a complete GEANT simulation of the detector and then embedded in actual ‘zero bias’ STAR events; this embedding procedure accurately accounts for the detector noise and backgrounds, including overlapping events recorded in the STAR TPC during its sizeable active time windows. As Fig. 2 shows, the agreement between the Monte Carlo and data is very good.

The efficiency depends only weakly on the pair mass and pair p_T , but depends fairly strongly on rapidity. The rapidity dependence has a bell shape with a maximum of 13% at $y \approx 0.1$. It is slightly asymmetric because of inefficiencies on one of the TPC West (rapidity < 0) sectors. A major uncertainty in the reconstruction efficiency stems from uncertainties in the actual (‘as-built’) positions of the TOF slats, which may not be completely accurately reflected in the simulations; this uncertainty may affect the measured $d\sigma/dy$, particularly at large rapidity; it does not significantly affect the pair p_T or mass acceptance uncertainties.

The two ZDC calorimeters detect the neutrons emitted by both beam in mutual electromagnetic dissociation with efficiency close to 100% and energy resolution sufficient to separate up to three neutron peaks. Figure 3 shows the ADC distribution from the West ZDC for events that satisfy a cut which selects events with a single neutron in the East ZDC and a photoproduced ρ^0 with $|y| < 1$ and $p_T < 100$ MeV/c.

This analysis considers two classes of nuclear breakup: single neutrons (1n), associated with Giant Dipole Resonance), or any number of neutrons (Xn), from a broad range of photonuclear interactions. Unfortunately, the trigger condition, requiring 1 to 4 neutrons, were chosen to maximize the photoproduction yield, and were only a subset of the full Xn spectrum. So, we used the 1n1n events to normalize the XnXn cross-section, based on the STARlight calculation of the cross-section ratio. We find the ratio of triggered events to those with single neutrons in each ZDC, using the fit results in Table 1, and use the STARlight ratio of XnXn to 1n1n events to normalize the overall cross-section scale.

The relative cross-sections in Table 1 decrease slowly with increasing neutron number; for example, the cross-section for the $2n1n + 1n2n$ (*i.e.* the two directional combinations to get 1 neutron in one direction, 2 is 0.83 of the 1n1n cross-section. This ratio is larger than is seen for mutual Coulomb dissociation, where one calculation has the $2n1n + 1n2n : 1n1n$ ratio around 0.6 [23] and another finds a ratio around 0.4, albeit at a slightly lower beam energy [24]. Some of this difference is because the requirement of ρ photoproduction selects events with smaller impact parameters, where the photon spectrum is harder [18].

3. The $\pi^+\pi^-$ Mass Spectrum and $d\sigma/dt$

Figure 4 shows the efficiency-corrected, background-subtracted invariant-mass of the pion pairs with $p_T < 100$ MeV/c. Events with dipion mass $M_{\pi\pi} > 600$ MeV/c² were initially fitted with a modified Söding parametrization [25] which included a relativistic Breit-Wigner resonance for the ρ^0 plus a flat direct

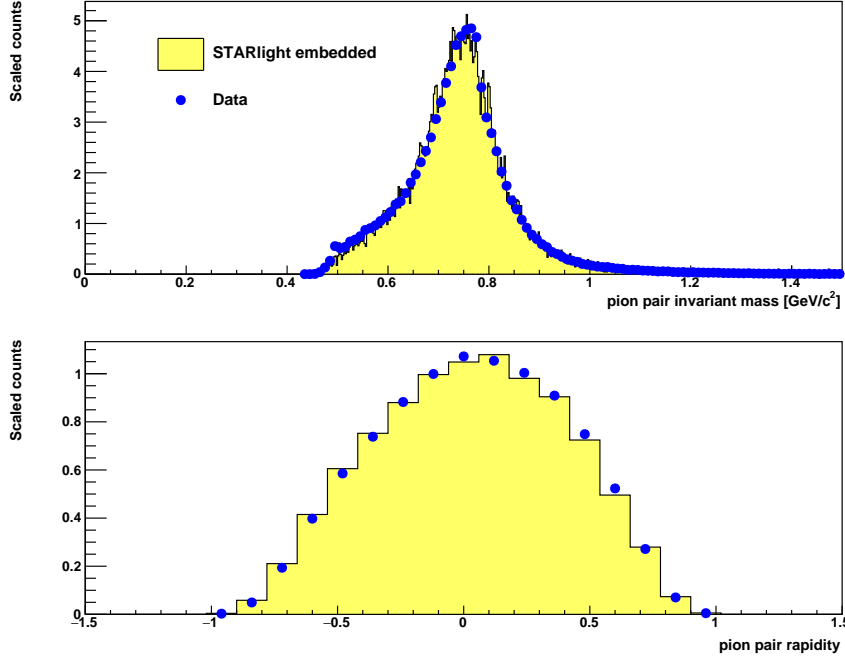


Figure 2: Comparison of uncorrected data (blue points) with embedded simulated ρ^0 and direct $\pi\pi$ events (yellow histogram). The simulated UPCs were run through a GEANT simulation of the detector, embedded in zero-bias background events, and subject to the same reconstruction programs as the data.

$\pi^+\pi^-$ continuum. This 2-component model was a poor fit to the data, so an additional relativistic Breit-Wigner component was added, to account for ω photoproduction, followed by its decay $\omega \rightarrow \pi^+\pi^-$. This leads to the following fit function:

$$\frac{d\sigma}{dM_{\pi^+\pi^-}} \propto \left| A_\rho \frac{\sqrt{M_{\pi\pi} M_\rho \Gamma_\rho}}{M_{\pi\pi}^2 - M_\rho^2 + i M_\rho \Gamma_\rho} + B_{\pi\pi} + C_\omega e^{i\phi_\omega} \frac{\sqrt{M_{\pi\pi} M_\omega \Gamma_{\omega \rightarrow \pi\pi}}}{M_{\pi\pi}^2 - M_\omega^2 + i M_\omega \Gamma_\omega} \right|^2 + f_p \quad (2)$$

where A_ρ is the ρ amplitude, $B_{\pi\pi}$ is for the direct pions and C_ω is for the ω . The momentum-dependent widths are taken to be

$$\Gamma_\rho = \Gamma_0 \frac{M_\rho}{M_{\pi\pi}} \left(\frac{M_{\pi\pi}^2 - 4m_\pi^2}{M_\rho^2 - 4m_\pi^2} \right)^{3/2} \quad (3)$$

and

$$\Gamma_\omega = \Gamma_0 \frac{M_\omega}{M_{\pi\pi}} \left(\frac{M_{\pi\pi}^2 - 9m_\pi^2}{M_\omega^2 - 9m_\pi^2} \right)^{3/2}, \quad (4)$$

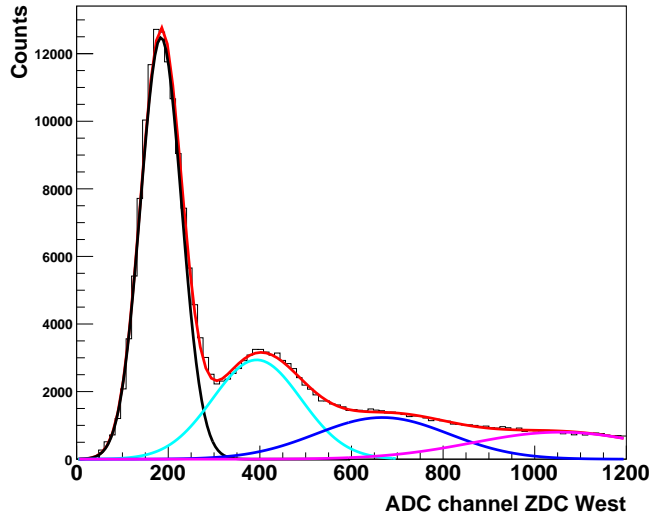


Figure 3: The shower energy in the West ZDC by neutron produced by mutual dissociation is shown as a distribution of ADC channels. These events had a single neutron detected on the East ZDC. The peaks corresponding to 1 to 4 neutrons are fitted with Gaussian distributions with standard deviations that grow as $n\sigma$ with n the number of neutrons and σ the standard deviation of the one neutron Gaussian. The red curve is the sum of all Gaussians which are also displayed individually. The quality of fit is $\chi^2/NDF = 498/88$. The large χ^2/NDF is due to the very small statistical errors and the imperfect descriptions of the neutron peaks. It does not introduce significant errors on the number of neutrons in each peak.

where Γ_0 is corresponding pole width for each meson. For the ω , the $9m_\pi^2$ term is because ω decay is dominated by the three-pion channel, assuming a phase space distribution. The branching ratio for $\omega \rightarrow \pi^+\pi^-$ is small, so we use

$$\Gamma_{\omega \rightarrow \pi\pi} = \sqrt{\text{Br}(\omega \rightarrow \pi\pi)} \Gamma_0 \frac{M_\omega}{M_{\pi\pi}} \left(\frac{M_{\pi\pi}^2 - 4m_\pi^2}{M_\omega^2 - 4m_\pi^2} \right)^{3/2} \quad (5)$$

with $\text{Br}(\omega \rightarrow \pi\pi) = 0.0153^{+0.11}_{-0.13}$ [26]. Here, f_p is a quadratic polynomial that describes the remaining remnant background. The masses and widths of the ρ and ω were allowed to float, making for a total of eleven parameters: four masses/widths, three amplitudes, the phase of the ω meson, and three parameters for the polynomial background.

In Fig. 4, the fitted ρ component is shown by the full blue line, with the direct $\pi\pi$ component shown in dashed black, the dashed blue line shows the interference between the two components. The full red line shows the fitted ω component and the dashed red line shows the interference between the ρ^0 and the ω components.

Table 2 shows the fit results. The ρ mass and width and the ω mass are in good agreement with their generally accepted values [26]. The ω considerably

	1n	2n	3n
1n	1.38 ± 0.24	0.57 ± 0.11	0.39 ± 0.07
2n	0.57 ± 0.11	0.23 ± 0.04	0.18 ± 0.03
3n	0.40 ± 0.07	0.19 ± 0.03	0.15 ± 0.03

Table 1: Mutual dissociation cross section (in mb) for events with exclusive coherent ρ^0 photoproduction. The row number shows the number of neutrons detected in the East ZDC and the column number lists the number of neutrons detected in the West ZDC. The cross sections are an average of two measurements: one of them uses the West ZDC to set the number of neutrons on that beam with ADC channel cuts defined by the dip between the 1 and 2 neutron peaks, and the other measurement has the East ZDC selecting events in similar manner. These two measurements differ in the off diagonal term and the systematic uncertainty on the selection of the number of neutrons in either ZDC is taken to be equal to the deviation from the average value. Statistical errors are small ($< 1\%$) and are not listed. Systematic errors arising from the cuts used to select the events added were added in quadrature to the sum in quadrature of the relevant common uncertainties listed in Tab. 3 (17%).

wider than the standard value, because it is broadened by the detector resolution. At the ω peak, the detector resolution is about $8.5 \text{ MeV}/c^2$. The fit $\chi^2/DOF = 314/297$ shows that the data and model are consistent, within the statistical errors.

The ratio of ρ to direct $\pi\pi$ amplitudes, $|B/A| = 0.78 \pm 0.01$ (*stat.*) ± 0.08 (*syst.*) $(\text{GeV}/c^2)^{-1/2}$ agrees, within errors, with the value reported in the previous STAR publication [10]: $(0.89 \pm 0.08$ (*stat.*) ± 0.09 (*syst.*)). The same ratio has been measured at the higher energy of the LHC (2.76 TeV per nucleon) by the ALICE collaboration [11] which finds a smaller value $(0.50 \pm 0.04$ (*stat.*) $_{-0.04}^{+0.10}$ (*syst.*)).

The ratio of ω to ρ amplitudes $C/A = 0.34 \pm 0.027$ (*stat.*) ± 0.04 (*syst.*). The ω amplitude is small, but the ω is clearly visible through its interference with the ρ . This interference produces a small kink in the spectrum just above $800 \text{ MeV}/c^2$. The ω amplitude agrees with a prediction from STARlight [7], $C/A = 0.32$ which uses the $\gamma p \rightarrow \omega p$ cross-section, and a classical Glauber calculation.

The only previous measurement of ρ - ω interference in the $\pi^+\pi^-$ channel is by a DESY-MIT group, using 5-7 GeV photon beams [27]. That fit used a similar, but not identical fit function, and found, neglecting differences in the treatment of the ω width, the $|C/A| = 0.36 \pm 0.04$ ($|C/A| = \zeta \sqrt{M_\rho \Gamma_\rho / M_\omega \Gamma_\omega} / \sqrt{Br(\omega \rightarrow \pi\pi)}$) in their terminology).

The fit finds a non-zero ω phase angle, $\phi_\omega = 1.73 \pm 0.13$ (*stat.*) ± 0.17 (*syst.*). Here, the systematic error is determined by varying the lower range of the fit to the $M_{\pi\pi}$ distribution between 520 and 600 MeV.

Our phase angle result is close to the DESY-MIT measurement of 1.68 ± 0.26 . This agreement is better than might be expected, since the DESY-MIT experiment used much lower energy photons, in a regime where production proceeds via both single meson and Pomeron exchange. Other experiments have studied ρ - ω interference using photoproduction to the e^+e^- final state, where the ω is more visible, but the branching ratios are much smaller, or via

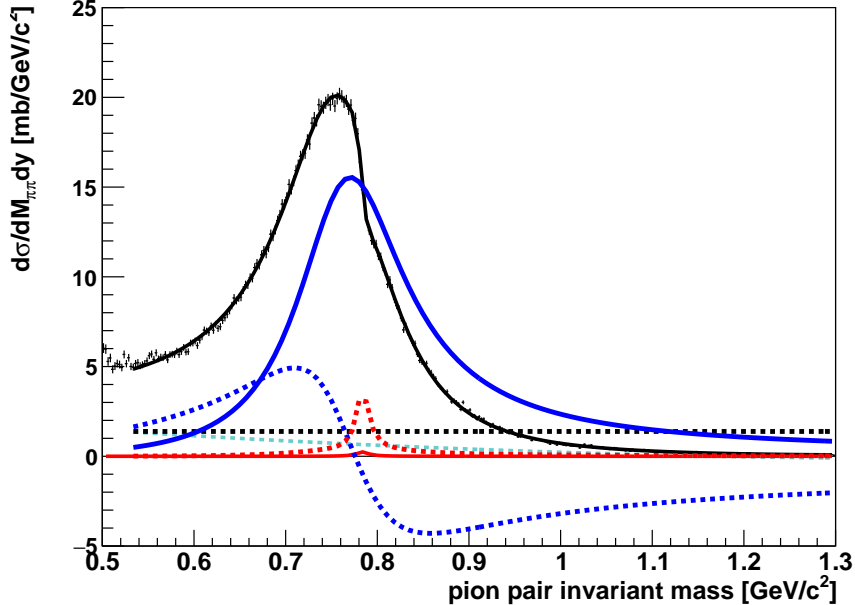


Figure 4: The $\pi^+\pi^-$ invariant-mass distribution for all selected $\pi\pi$ candidates with $p_T < 100$ MeV/c. The black markers show the data (in 2.5 MeV/ c^2 bins). The black curve is the modified Söding fit to the data in the range $0.53 < M_{\pi\pi} < 1.3$ GeV. The ρ^0 Breit-Wigner component of the fitted function is shown with a blue curve and the constant non-resonant pion pair component is displayed with a black-dashed one. The interference between non-resonant pion pairs and the ρ^0 meson is shown with a blue-dashed curve. The Breit-Wigner distribution for the ω mesons is shown with a red curve and the interference between ρ^0 and ω is shown with a red-dashed curve. A small second order polynomial shown with a cyan-dashed curve accounts for the remnant background.

the reaction $e^+e^- \rightarrow \pi^+\pi^-$, and found similar phase angles [28].

An alternate fit was performed, where $B_{\pi\pi}$ was multiplied by a mass dependent term, $M_{\pi\pi}/M_\rho[(M_{\pi\pi}^2/4 - m_\pi^2)/(M_\rho^2/4 - m_\pi^2)]^{3/2}$ to account for possibility that the continuum $\pi\pi$ pairs do not completely interfere with the ρ or ω . This fit produced similar results, but with a slightly worse χ^2/DOF .

To study the photon energy dependence of the amplitude ratios, we performed the fit in five bins of rapidity: $|y| < 0.15$, $0.15 < |y| < 0.35$, and $|y| > 0.35$. The amplitudes should be symmetric around $y = 0$; pairing by $|y|$ provides a check on rapidity-dependent systematic errors.

The rapidity is related to photon energy k , with, at low p_T , in the lab frame, $k = M_{\pi\pi}/2 \exp(\pm y)$, with the \pm sign because of the two-fold ambiguity as to which nucleus emitted the photon. Away from $y = 0$, the cross section is dominated by the lower photon energy. With this assumption, $y=0$ corresponds to photon energy $k = 380$ MeV/c in the lab frame, $k = 82$ GeV in the target nucleus frame and center of mass energy 12.4 GeV. $|y| = 0.15$ corresponds to

Fit Parameter	value	units
M_ρ	0.7757 ± 0.0006	GeV/c ²
Γ_ρ	0.1475 ± 0.0014	GeV/c ²
A_ρ	1.511 ± 0.005	
$B_{\pi\pi}$	-1.176 ± 0.016	(GeV/c ²) ^{-1/2}
C_ω	0.5108 ± 0.0408	
M_ω	0.7838 ± 0.0009	GeV/c ²
Γ_ω	0.0163 ± 0.0017	GeV/c ²
ϕ_ω	1.73 ± 0.13	radians
$f_p p_0$	3.566 ± 0.304	
$f_p p_1$	-5.084 ± 0.53	
$f_p p_2$	1.743 ± 0.24	

Table 2: Results of fitting Eq. 2 to the data. Three parameters p_0 , p_1 and p_2 are for the the polynomial background.

$k=327$ MeV/c in the lab frame, 71 GeV photon energy in the target nucleus frame and 11.5 GeV center of mass energy, while $|y|=0.35$ corresponds to 267 MeV (58 GeV photon energy in the target frame), and 10.4 GeV center of mass energy.

These bins were chosen so that each bin had close to 100,000 pion pairs. To ensure the fits were stable, the values of M_ω and Γ_ω were fixed to the values extracted from the fit to the rapidity integrated pion pair mass distribution. Figure 5 shows the ratios $|B/A|$ and C/A in the five bins in rapidity. Both $|B/A|$ and C/A are, within the total errors, flat as rapidity varies, showing that these ratios do not have a large dependence on the photon energy.

To determine the ρ^0 cross-section as a function of rapidity, for each bin, we find the integral of the ρ Breit-Wigner function for masses ranging from $2M_\pi$ and $M_\rho + 5\Gamma_\rho$. We also determine a correction factor, the ratio of the number of ρ^0 to the total number of $\pi^+\pi^-$, which is used for the remaining results discussed here.

Figure 6 shows the acceptance corrected distribution of ρ^0 mesons detected in events with only two tracks from the triggered vertex. The asymmetry between positive and negative rapidity gives a measure of the rapidity-dependent systematic uncertainties in the cross section. These are likely due to asymmetries in the as-built location of the TOF counters. The magnitude of this uncertainty grows slowly from mid-rapidity to reach a value of 4% at $y = 0.7$. Since the actual lengths of the TOF slats are known, this uncertainty does not apply for rapidity-integrated measurements.

The systematic uncertainties in these measurements fall into two classes, either an overall scale factor on the cross-section, or point-to-point. The overall scale factor is usually dominant.

The scaling from the rapidity distribution extracted from 1n1n events to the previously measured XnXn distribution uses a correction, extracted from the event generator STARLight and introduces a 6% uncertainty related to the

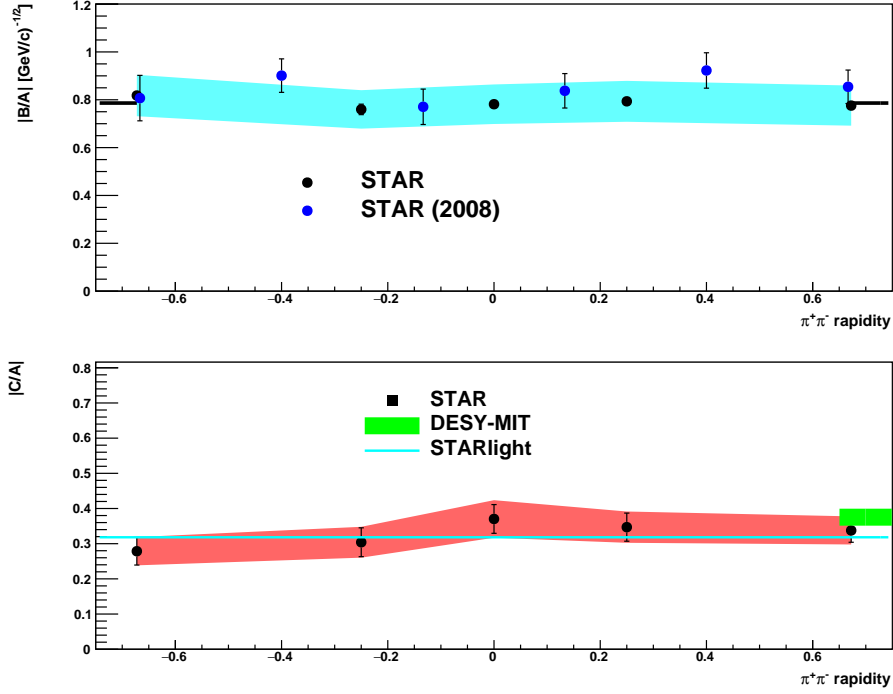


Figure 5: (Top) The ratio $|B/A|$ of amplitudes of non-resonant $\pi^+\pi^-$ and ρ^0 mesons. The black points (with shaded blue systematic error band) are from the current analysis, while the previous STAR results are shown with blue-filled circles. The thick black line shows the rapidity-averaged result. In the bottom panel, the black points show the ratio $|C/A|$ of the ω to ρ^0 amplitude. The red band shows the systematic errors, while the horizontal blue line shows the STARlight prediction and the most recent branching ratio for $\omega \rightarrow \pi^+\pi^-$ decay [26]. The green band shows the DESY-MIT result for $|C/A|$ [27]. This result was at much lower photon energies leads to a large effective rapidity. For the lower energy photon solution of the two-fold ambiguity, the effective rapidity would be about 2.5.

uncertainty in the neutron data used as input to STARlight, squared because we detect neutrons in both beams. This uncertainty applies only to the X_nX_n results.

The uncertainty in the integrated luminosity is 10%, as with previous measurements [10] mainly driven by the fraction of the total Au+Au cross section accessible with the trigger used to collect this data.

The selection of the number of neutrons produced in mutual electromagnetic dissociation is based on the ZDC calorimeters response. We allocate a 5% uncertainty to this neutron counting due to small non-linearities in the calorimeters and overlaps between one and many neutron distributions.

We assign a 7% uncertainty due to modelling of the TOF system in the simulation.

The track reconstruction efficiency for the STAR TPC has a 3% per track

<i>Name</i>	Value	Comment
Luminosity	10.0%	
STARLight model	6.0%	only for XnXn results
ZDC	5.0%	ADC ch. to num. neutrons
TOF geometry modeling	7.0%	
TPC tracking efficiency	6.0%	3% per track [20]
Vertex Finder efficiency	5.0%	Background driven
BBC veto in trigger	2.0%	Background driven
Efficiency determination	7.0%	Ev. Gen., Material budget
Background subtraction	1.5%	
Quadrature Sum	18.1%	

Table 3: Summary of all common systematic uncertainties identified in the generation of the rapidity distribution shown in Fig. 6 and the $-t$ distributions shown in Figs. 7 and 8. All these uncertainties are presented as a percent fractions of the measured quantities.

uncertainty, for a total of 6% [20] while the efficiency of the vertex finder is known with a 5% uncertainty, driven by the effect of backgrounds.

The uncertainty in how often the BBC detectors will veto good UPC events is due to fluctuating backgrounds. Even with use of embedding techniques, we estimate that these veto conditions introduce a 2% uncertainty to the results.

The same-sign pion pair distributions are the best estimators for the background for these two track events. The background subtraction was done at the level of raw histograms or after a fit to the background to eliminate statistical fluctuations. The relative deviation between those two procedures found in the fully corrected distributions is found to be 1.5%.

Summing these systematic uncertainties in quadrature leads to a 18.1% overall common uncertainty. This uncertainty is a bit higher than in our comparable previous publication [10], largely because of additional uncertainties associated with the pileup and the more complex trigger and which is required to deal with the higher luminosities. Table 3 summarizes all the common systematic uncertainties identified in this measurement.

The main point-to-point systematic uncertainties in the rapidity and p_T distributions come from the track selection and particle identification. The systematic uncertainties were evaluated by varying the track quality cuts and PID cuts around their central value in both the data and simulation, and seeing how the final results varies. Table 4 lists the uncertainties in the rapidity distribution while Table 5 list the point-to-point uncertainties for the p_T distribution.

The ALICE collaboration has also studied ρ photoproduction, in lead-lead collisions at the Large Hadron Collider (LHC) [11]. They fit their dipion mass distribution in the range from 0.6 to 1.5 GeV² to a function like Eq. 2, but without the ω component, finding masses and widths consistent with the standard values. Their cross-section values, $d\sigma/dy$ were about 10% above the STARlight prediction.

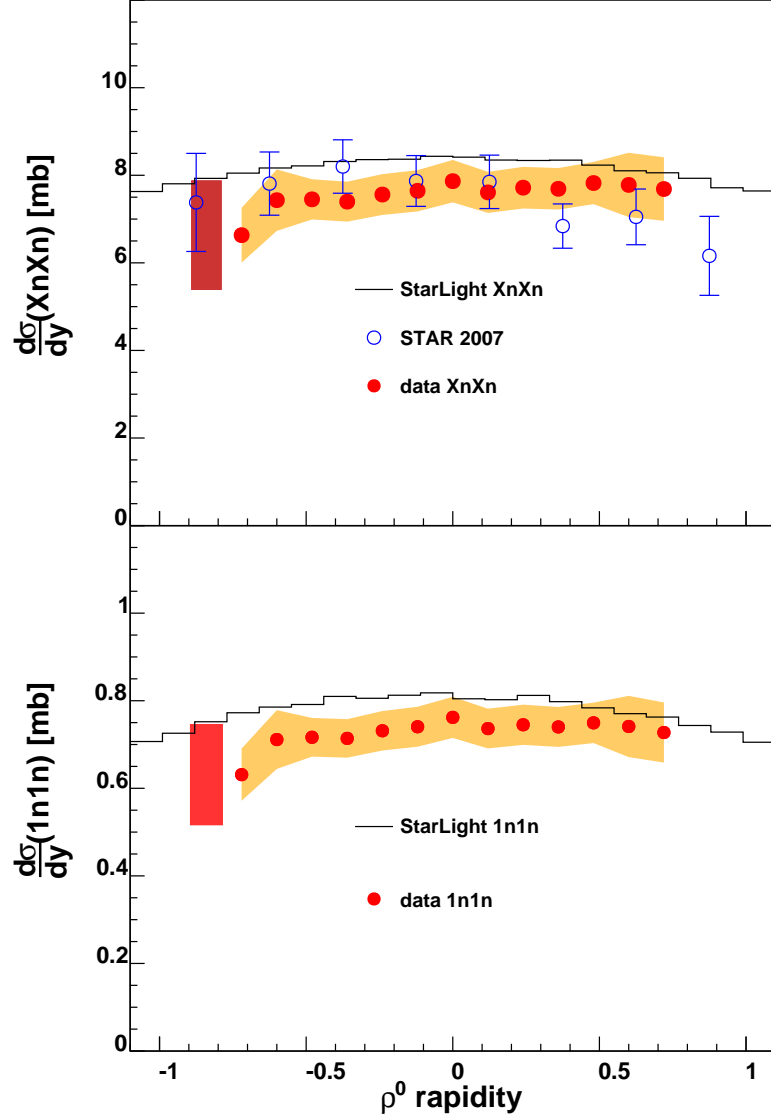


Figure 6: $d\sigma/dy$ for exclusively photoproduced ρ^0 mesons in (top) XnXn events and (bottom) 1n1n events. The data are shown with red markers. The statistical errors are smaller than the symbols, the orange band shows the quadrature sum of the point-to-point systematic uncertainties. The red box at $y \sim -0.9$ shows the quadrature sum of the common systematic uncertainties. The black histograms are the STARlight calculation for ρ^0 mesons with mutual dissociation. The blue markers in the top panel show the previous STAR measurement [10].

Rapidity	PID cut	Fit to eff.	Number of track hits	TOF asymmetry
-0.70, -0.5	8.%	0.25%	0.2%	5%
-0.5, 0.	5.%	0.25%	0.05%	3.6%
0., 0.5	5.%	0.25%	0.05%	3.6%
0.5 - 0.7	8.%	0.25%	0.2%	5%

Table 4: Point-to-point systematic uncertainties on $d\sigma/dy$ (Fig. 6), as a percent of the measured cross section in four rapidity ranges. PID cut refers to uncertainty in the efficiency for π identification via the truncated dE/dx [29]. Those cuts were varied simultaneously in the data and simulation to determine the uncertainty due to particle identification. The fit to efficiency is the uncertainty in the parameterization of the efficiency, while the number of track hits refers to the minimum number of points used for fitting the track. The TOF asymmetry is the uncertainty due to the positions of the TOF slats. The actual $d\sigma/dy$ is symmetric around $y = 0$; the observed asymmetry is as a measure of the systematic uncertainty from the TOF system.

4. $d\sigma/dt$

Figure 7 shows the differential cross section $d\sigma/dt$ for ρ^0 mesons with all rapidities within the measured range $|y| < 1$, after like-sign background subtraction, with t the Mandelstam variable $t = t_{\parallel} + t_{\perp}$ with $t_{\parallel} = -M_{\rho}^2/(\gamma^2 e^{\pm y})$ almost negligible and $t_{\perp} = -(p_T^{pair})^2$. The number of ρ^0 mesons is obtained from a simple scaling by a common factor of 0.75 extracted from comparisons between the number of pion pairs with invariant masses ranging from 500 MeV/ c^2 to 1.5 GeV/ c^2 and the integral of the ρ^0 Breit-Wigner function extracted from fits in rapidity and $-t$ bins. In all comparisons, the integrals are performed from $2M_{\pi}$ to $M_{\rho} + 5\Gamma_{\rho}$. The yield of ρ^0 mesons is also corrected for the compounded effects of tracking reconstruction and geometrical acceptance, vertex finding efficiency and the finite track and TOF detector matching efficiency extracted from the embedded simulations. This correction is flat in t and has an average value of 6.4% over all rapidity values. Finally the distribution is normalized by the luminosity integrated over all data runs used in this analysis. The large peak in $d\sigma/dt$ for $|t| < 0.1\text{GeV}^2$ is expected from coherent photoproduction. At substantially larger $|t|$, production should be dominated by incoherent interactions with individual nucleons in the target ion. At still higher $|t|$ (not seen here), individual partons should play a role.

We separate the ρ^0 t spectrum into coherent and incoherent components based on the shape of the distribution in Fig. 7. Because of the neutron requirement in the trigger, and the presence of Coulomb excitation, we cannot use the presence of neutrons from nuclear breakup as an event-by-event sign of incoherence [30].

The incoherent component is fit with the so called ‘‘dipole’’ form factor

$$\frac{d\sigma}{dt} = \frac{A/Q_0^2}{(1 + |t|/Q_0^2)^2} \quad (6)$$

used to describe low Q^2 photon-nucleon interactions [31]. The fit range for the XnXn events starts at $-t = 0.2\text{ GeV}^2$ (above the coherent production region) and

extends to $-t = 0.45 \text{ GeV}^2$ as shown by the black curve in the figure. The upper limit in t is chosen to reduce the contamination from hadronic interactions. For the events with mutual dissociation into any number of neutrons (XnXn), the fit finds $A = 3.46 \pm 0.02$, $Q_0^2 = 0.099 \pm 0.015 \text{ (GeV/c)}^2$, with $\chi^2/NDF = 19/10$. For events with mutual dissociation into single neutrons (1n1n), the fit parameters are: $A = 0.191 \pm 0.003$, $Q_0^2 = 0.099$ (fixed) (GeV/c)^2 , with $\chi^2/NDF = 13.7/10$. The integral of the fit to the incoherent component in the XnXn events results in a value of cross section $\sigma_{incoh} = 2.89 \pm 0.02 \text{ (stat.)} \pm 0.03 \text{ (syst.)}$ mb. The integral of the coherent component discussed below amounts to $6.49 \pm 0.01 \text{ (stat.)} \pm 0.01 \text{ (syst.)}$ mb. The incoherent component of the distribution extracted from 1n1n events is fitted to the same function as the XnXn distribution. The range of $-t$ and rapidity values are also the same. The integral of the fit to the incoherent component in the 1n1n events results in a value of cross section $\sigma_{incoh} = 0.162 \pm 0.01 \text{ (stat.)} \pm 0.005 \text{ (syst.)}$ mb. The integral of the 1n1n coherent component amounts to $0.7696 \pm 0.004 \text{ (stat.)} \pm 0.004 \text{ (syst.)}$ mb.

The corresponding ratios are:

$$\begin{aligned} \sigma_{incoherent}^{XnXn} / \sigma_{coherent}^{XnXn} &= 0.445 \pm 0.003 \text{ (stat.)} \pm 0.005 \text{ (syst.)} \\ \sigma_{incoherent}^{1n1n} / \sigma_{coherent}^{1n1n} &= 0.233 \pm 0.014 \text{ (stat.)} \pm 0.007 \text{ (syst.)}. \end{aligned}$$

The difference in the ratio found for 1n1n and XnXn collision is somewhat larger than the previous STAR analysis [10], particularly in the XnXn channel. The ratio difference could come from a variety of sources. First, at large $|t|$, it is possible for a single photon to both produce a ρ^0 and leave the target nucleus excited, breaking the assumed factorization paradigm. The rate has not been calculated for ρ^0 , but for J/ψ , the cross-section is significant [32]. The calculated cross-section for vector meson production with excitation is very low for single neutron emission, so this would alter the XnXn cross-section ratio more than the 1n1n.

Second, unitarity corrections could play a role by changing the impact parameter distributions for 1n1n and XnXn interactions. Near grazing incidence, the cost of introducing another low-energy photon into the reaction is small. So, one photon can excite a nucleus, for example to a GDR, while a second photon can excite the nucleus further, leading to Xn emission rather than 1n [33]. The additional photon alters the impact parameter distributions for the 1n1n and XnXn channels; the XnXn channel will experience a slightly larger reduction at small $|t|$ due to interference from the two production sites; this may lead to slightly different measured slopes and coherent/incoherent ratios. These probabilities are included in STARlight [19]. There may also be a shift due to a larger non-uniform photon illumination of the target nucleus.

The coherent component of the t distribution is then extracted by a subtracting the incoherent-component power law fit from the total $d\sigma/dt$. The resulting differential cross section for ρ^0 photoproduction accompanied with mutual dissociation of the nuclei into any number of neutrons (XnXn) and only one neutron (1n1n) is shown in Fig. 8 with red and black markers respectively. In both 1n1n and XnXn events, two well defined minima can clearly be seen.

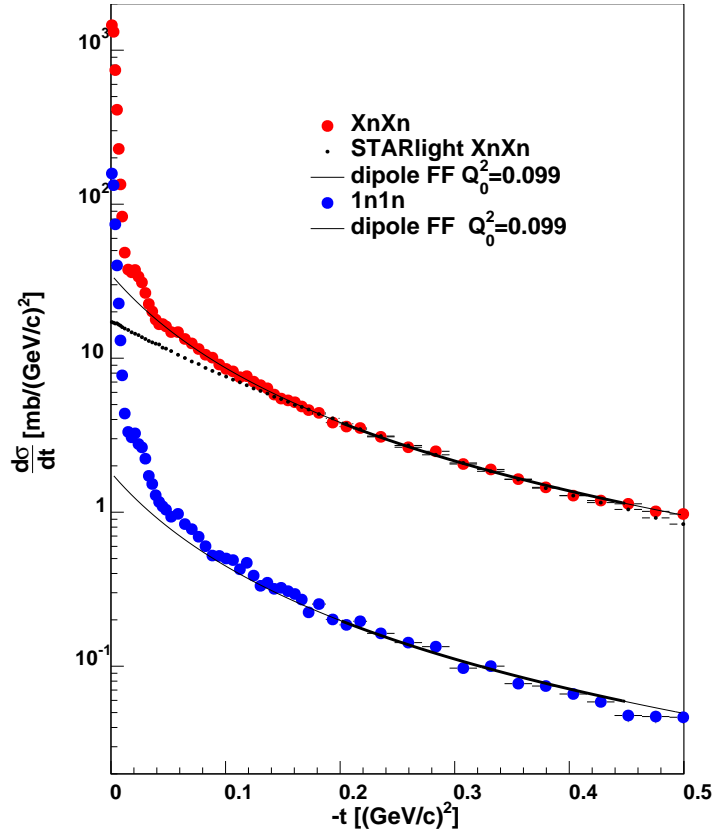


Figure 7: The $-t$ distribution for exclusive ρ^0 mesons in events with 1n,1n mutual dissociation (blue markers) or XnXn (red markers). The high t part of those distributions, which is dominated by the contribution from incoherent interactions is fit to a dipole form factor, shown with a thin line. The STARlight prediction for the incoherent contribution is shown by the histogram with small black markers.

$-t[(\text{GeV}/c)^2]$	track sel.	pion PID	Incoh. comp. sub.
0 - 0.02	0.2%	8%	0.5%
0.02 - 0.04	0.2%	8%	3.0%
0.04 - 0.1	0.2%	8%	8.5%

Table 5: Point-to-point systematic uncertainties for the $-t$ distribution shown in Fig. 8, as a per-cent of the measured cross section in three $-t$ ranges. The PID and track selection uncertainties are described in the text. The uncertainty in the incoherent component subtraction was estimated by selecting the biggest relative deviation from the default value and cross sections extracted by changing the value of the fit parameters by one standard deviation while the other parameters remain at the default fit value.

In both spectra, the first minima is at $-t = 0.018 \pm 0.005 (\text{GeV}/c)^{-2}$. A second minima is visible at $0.043 \pm 0.01 (\text{GeV}/c)^{-2}$. To first order, the gold nuclei are beginning to show signs of acting like black disks, with similar behavior for 1n1n and XnXn interactions.

A similar first minimum may be visible in ALICE data. Figure 3 of ref [11] shows an apparent dip in dN/dp_T for ρ photoproduction, around $p_T = 0.12 \text{ GeV}/c$ ($-t = 0.014 \text{ GeV}^2$). This is for lead-lead collisions; lead is slightly larger than gold, so the dip should be at smaller t .

These minima are shallower than would be expected for $\gamma - A$ scattering, because the photon p_T partly fills in the dips in the $\gamma - A$ p_T spectrum. There are several theoretical predictions about the location and depth of these dips. One of them found the correct depths, but slightly different locations [34]. The calculation that used a quantum Glauber calculation along with nuclear shadowing did a better job of predicting the locations of the first minimum [13], although that calculation did not include the photon p_T , so missed the depth of the minimum. The *sartre* event generator run in UPC mode at RHIC energies [36] produces a Au nuclei recoil after ρ^0 elastic scattering with a remarkable agreement with the ρ^0 t distribution presented here.

An exponential function is used to characterize the spectrum below the first peak ($0.0024 < |t| < 0.0098 (\text{GeV}/c)^2$). There, the measured slope is $426.4 \pm 1.8 (\text{GeV}/c)^{-2}$ for the XnXn events and $407.8 \pm 3.2 (\text{GeV}/c)^{-2}$ for the 1n1n events. The XnXn slope is very similar to the ALICE measurement of $426 \pm 6 \pm 15 (\text{GeV}/c)^{-2}$ [11]; there is no evidence for an any increase in effective nuclear size with increasing photon energy.

At very small t , $|t| < 10^{-3} \text{ GeV}^2$, both cross section flatten out and turn downward, as can be seen in the insert in Fig. 8. This is expected due to destructive interference between ρ production on the two nuclear targets [34, 35].

The systematic uncertainties on this differential cross-section come in two types, common uncertainties, from Tab. 3, and point-to-point uncertainties described above and listed in Table 5. The green and red bands in Fig. 8 are the sum in quadrature of all systematic uncertainties and statistical errors.

The shape of $d\sigma/dt$ for coherent photoproduction is determined by the position of the interaction sites within the target, and one can, in principle, determine the density distribution of the gold nucleus via a two dimensional Fourier

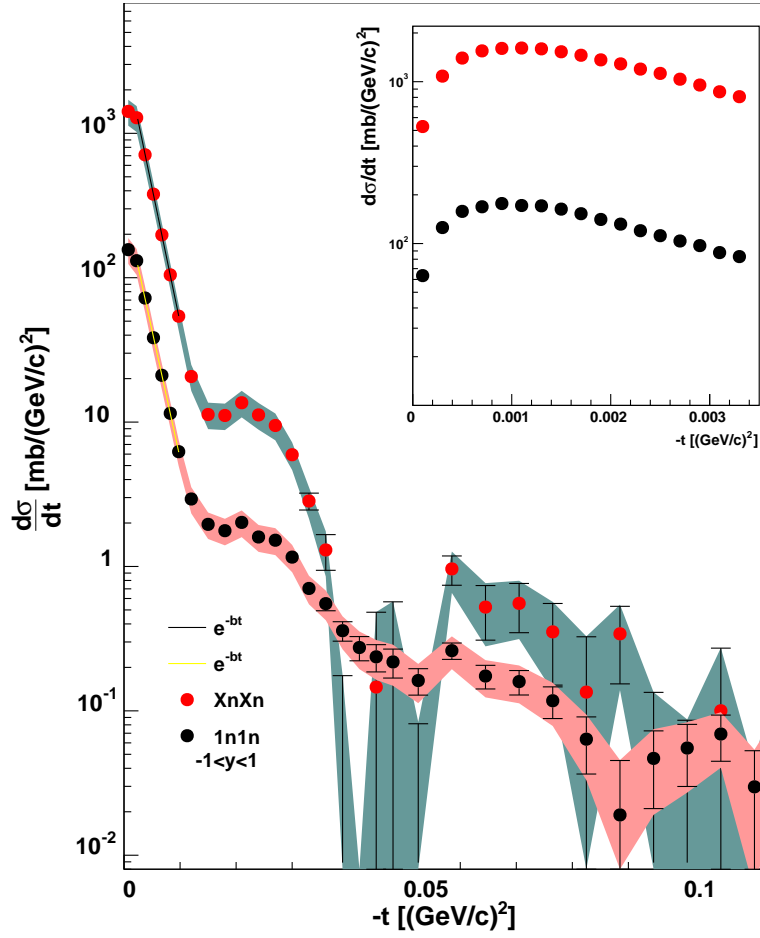


Figure 8: Fully normalized coherent diffraction patterns for ρ^0 mesons detected in exclusive XnXn events is shown with red markers. The same distribution but extracted from 1n1n events is shown with black markers. The filled bands shows the sum in quadrature of all systematic uncertainties listed in table 4 and the statistical errors, which are shown as vertical lines. The insert shows, with finer binning at low p_T , the effects of the destructive interference between photoproduction with the photon emitted by any of the two ions.

transform of $d\sigma/dt$. The beam energies at RHIC are high enough so that, for ρ photoproduction at mid-rapidity, the longitudinal density distribution may be neglected and the ions may be treated as discs. Nuclei are azimuthally symmetric, so the radial distribution may be determined with a one-dimensional Fourier-Bessel (Hankel) transformation:

$$F(b) \propto \frac{1}{2\pi} \int_0^\infty dp_T p_T J_0(bp_T) \sqrt{\frac{d\sigma}{dt}} \quad (7)$$

Figure 9 shows the result of a numerical calculation of this transform in the region $|t| < 0.06 \text{ GeV}^2$. The tails of $F(b)$ are negative around $|b|=10 \text{ fm}$. This may be due to interference between the two nuclei. The decrease in $d\sigma/dt$ at very small t is due to what is effectively a negative amplitude coming in from the ‘other’ nucleus [35].

We varied the maximum t used for the transform over the range 0.05 to 0.09 GeV^2 ; this led to substantial variation at small b , shown by the cyan region in Fig. 9. The origin of this variation is not completely clear, but it may be related to aliasing due to the lack of a windowing function [37], or because of the limited statistics at large t . There is much less variation at the edges of the distribution. This leads us to believe that the transform can be used in the region where b ranges from $\sim 4 - 7 \text{ fm}$. In this region, we determine the full-width half-maximum (FWHM) of the distribution to be $2 \times (6.17 \pm 0.12) \text{ fm}$. This FWHM is a measure of the hadronic size of the gold nucleus. With theoretical input, it could be compared with the electromagnetic (proton) radius of gold, as determined by electromagnetic scattering. The difference would be a measure of the neutron skin thickness of gold, something that is the subject of considerable experimental interest [38, 39].

Because of the possibility of ρ absorption the p_T introduced by the photon, the non-uniformity of the photon field (it is stronger on the ‘near’ side of the nucleus) and the effect of interference between the two production sites, care must be used in interpreting the transform.

5. Summary and conclusion

In conclusion, STAR has made a precision study of ρ , ω and direct $\pi^+\pi^-$ photoproduction in 200 $\text{GeV}/\text{nucleon}$ gold-on-gold ultra-peripheral collisions, using 394,000 $\pi^+\pi^-$ pairs.

We fit the invariant mass spectrum to a mixture of ρ , ω and direct $\pi^+\pi^-$ (including interference terms). The ratio of ρ to direct $\pi\pi$ is similar to that in previous measurements, while the newly measured ω contribution is comparable with predictions based on the previously measured $\gamma p \rightarrow \omega p$ cross section and the $\omega \rightarrow \pi^+\pi^-$ branching ratio. The relative fractions of ρ , ω and direct $\pi^+\pi^-$ do not vary significantly with rapidity, indicating that they all have a similar dependence on photon energy.

We also measure the cross section $d\sigma/dt$ over a wide range, and separate out coherent and incoherent components. The coherent contribution exhibits

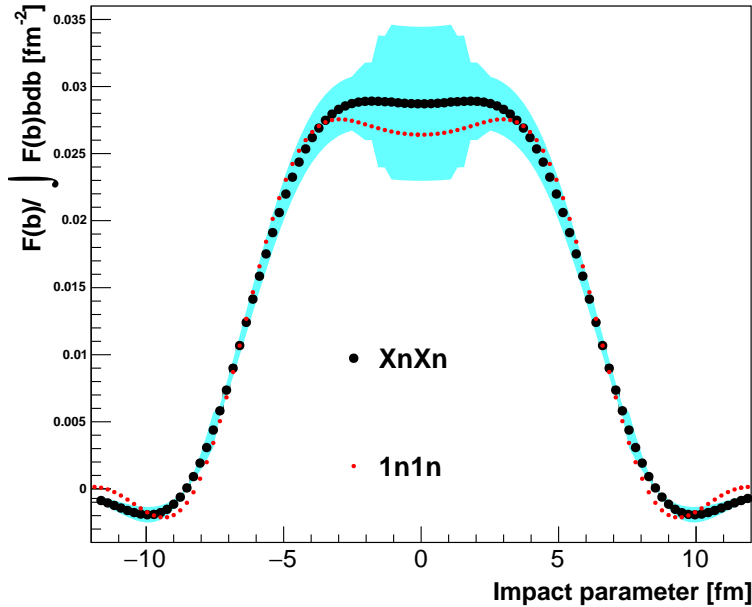


Figure 9: The normalized nucleon distribution in the transverse plane, the result of a two-dimensional Fourier transform (Hankel transform) of the XnXn and 1n1n diffraction patterns shown in Fig. 8. The integration is limited to a region where data is available; in the range $0 < |t| < 0.06 \text{ GeV}^2$. The cyan error band shows the effect of changing the maximum t to 0.05, 0.07 and 0.09 GeV^2 . In order to highlight the similarity of both results at their falling edges, the resulting histograms are scaled by their integrals from -12 to 12 fm. The FWHM of both transforms is $2 \times (6.17 \pm 0.12) \text{ fm}$ consistent with the coherent diffraction of ρ^0 mesons off an object as big as the Au nuclei.

multiple diffractive minima, indicating that the nucleus is beginning to act like a black disk.

This measurement provides a nice lead-in to future studies of photo- and electro- production at an electron-ion collider (EIC) [40], where nuclei may be probed with photons at a wide range of Q^2 [41].

6. Acknowledgments

References

- [1] G. Baur, K. Hencken, D. Trautmann, S. Sadovsky, Y. Kharlov, Coherent gamma gamma and gamma-A interactions in very peripheral collisions at relativistic ion colliders, Phys.Rept. 364 (2002) 359–450. [arXiv:hep-ph/0112211](https://arxiv.org/abs/hep-ph/0112211), doi:10.1016/S0370-1573(01)00101-6.

- [2] C. A. Bertulani, S. R. Klein, J. Nystrand, Physics of ultra-peripheral nuclear collisions, *Ann. Rev. Nucl. Part. Sci.* 55 (2005) 271–310. [arXiv:nucl-ex/0502005](#), [doi:10.1146/annurev.nucl.55.090704.151526](#).
- [3] J. Crittenden, Exclusive production of neutral vector mesons at the electron - proton collider HERA [arXiv:hep-ex/9704009](#).
- [4] S. Nussinov, Colored-quark version of some hadronic puzzles, *Phys. Rev. Lett.* 34 (1975) 1286–1289. [doi:10.1103/PhysRevLett.34.1286](#).
URL <http://link.aps.org/doi/10.1103/PhysRevLett.34.1286>
- [5] F. E. Low, Model of the bare pomeron, *Phys. Rev. D* 12 (1975) 163–173. [doi:10.1103/PhysRevD.12.163](#).
URL <http://link.aps.org/doi/10.1103/PhysRevD.12.163>
- [6] J. Bartels, K. J. Golec-Biernat, H. Kowalski, A modification of the saturation model: DGLAP evolution, *Phys. Rev. D* 66 (2002) 014001. [arXiv:hep-ph/0203258](#), [doi:10.1103/PhysRevD.66.014001](#).
- [7] S. R. Klein, J. Nystrand, Exclusive vector meson production in relativistic heavy ion collisions, *Phys. Rev. C* 60 (1999) 014903. [doi:10.1103/PhysRevC.60.014903](#).
URL <http://link.aps.org/doi/10.1103/PhysRevC.60.014903>
- [8] G. Agakishiev, et al., ρ^0 Photoproduction in AuAu Collisions at $\sqrt{s_{NN}}=62.4$ GeV with STAR, *Phys. Rev. C* 85 (2012) 014910. [arXiv:1107.4630](#), [doi:10.1103/PhysRevC.85.014910](#).
- [9] C. Adler, et al., Coherent ρ^0 production in ultraperipheral heavy ion collisions, *Phys. Rev. Lett.* 89 (2002) 272302. [arXiv:nucl-ex/0206004](#), [doi:10.1103/PhysRevLett.89.272302](#).
- [10] B. I. Abelev, et al., ρ^0 Photoproduction in Ultra-Peripheral Relativistic Heavy Ion Collisions with STAR, *Phys. Rev. C* 77 (2008) 034910. [arXiv:0712.3320](#), [doi:10.1103/PhysRevC.77.034910](#).
- [11] J. Adam, et al., Coherent ρ^0 photoproduction in ultra-peripheral Pb–Pb collisions at $\sqrt{s_{NN}} = 2.76$ TeV [arXiv:1503.09177](#).
- [12] L. Frankfurt, M. Strikman, M. Zhalov, Predictions of the generalized Glauber model for the coherent rho production at RHIC and the STAR data, *Phys. Rev. C* 67 (2003) 034901. [arXiv:hep-ph/0210303](#), [doi:10.1103/PhysRevC.67.034901](#).
- [13] L. Frankfurt, V. Guzey, M. Strikman, M. Zhalov, Nuclear shadowing in photoproduction of ρ mesons in ultraperipheral nucleus collisions at RHIC and the LHC [arXiv:1506.07150](#).

- [14] V. P. Goncalves, M. V. T. Machado, Photoproduction of ρ^0 meson in ultraperipheral heavy ion collisions at the BNL RHIC and CERN LHC, *Phys. Rev. C* 80 (2009) 054901. [arXiv:0907.4123](#), [doi:10.1103/PhysRevC.80.054901](#).
- [15] G. Sampaio dos Santos, M. V. T. Machado, Light vector meson photoproduction in hadron-hadron and nucleus-nucleus collisions at energies available at the CERN Large Hadron Collider, *Phys. Rev. C* 91 (2) (2015) 025203. [arXiv:1407.4148](#), [doi:10.1103/PhysRevC.91.025203](#).
- [16] M. Klusek-Gawenda, A. Szczurek, $\pi^+\pi^-$ and $\pi^0\pi^0$ pair production in photon-photon and in ultraperipheral ultrarelativistic heavy ion collisions, *Phys. Rev. C* 87 (5) (2013) 054908. [arXiv:1302.4204](#), [doi:10.1103/PhysRevC.87.054908](#).
- [17] B. L. Berman, S. C. Fultz, Measurements of the giant dipole resonance with monoenergetic photons, *Rev. Mod. Phys.* 47 (1975) 713–761. [doi:10.1103/RevModPhys.47.713](#).
URL <http://link.aps.org/doi/10.1103/RevModPhys.47.713>
- [18] G. Baur, K. Hencken, A. Aste, D. Trautmann, S. R. Klein, Multiphoton exchange processes in ultraperipheral relativistic heavy ion collisions, *Nucl. Phys. A* 729 (2003) 787–808. [arXiv:nucl-th/0307031](#), [doi:10.1016/j.nuclphysa.2003.09.006](#).
- [19] A. J. Baltz, S. R. Klein, J. Nystrand, Coherent vector meson photoproduction with nuclear breakup in relativistic heavy ion collisions, *Phys. Rev. Lett.* 89 (2002) 012301. [arXiv:nucl-th/0205031](#), [doi:10.1103/PhysRevLett.89.012301](#).
- [20] M. Anderson, et al., The Star time projection chamber: A Unique tool for studying high multiplicity events at RHIC, *Nucl.Instrum.Meth. A* 499 (2003) 659–678. [arXiv:nucl-ex/0301015](#), [doi:10.1016/S0168-9002\(02\)01964-2](#).
- [21] W. J. Llope, The large-area time-of-flight upgrade for STAR, *Nucl. Instrum. Meth. B* 241 (2005) 306–310. [doi:10.1016/j.nimb.2005.07.089](#).
- [22] C. Adler, A. Denisov, E. Garcia, M. Murray, H. Strobele, S. White, The RHIC zero-degree calorimeters, *Nucl. Instrum. Meth. A* 499 (2003) 433–436. [doi:10.1016/j.nima.2003.08.112](#).
- [23] I. A. Pshenichnov, J. P. Bondorf, I. N. Mishustin, A. Ventura, S. Masetti, Mutual heavy ion dissociation in peripheral collisions at ultrarelativistic energies, *Phys. Rev. C* 64 (2001) 024903. [arXiv:nucl-th/0101035](#), [doi:10.1103/PhysRevC.64.024903](#).
- [24] M. Klusek-Gawenda, M. Ciemala, W. Schafer, A. Szczurek, Electromagnetic excitation of nuclei and neutron evaporation in ultrarelativistic ultraperipheral heavy ion collisions, *Phys. Rev. C* 89 (5) (2014) 054907. [arXiv:1311.1938](#), [doi:10.1103/PhysRevC.89.054907](#).

- [25] P. Soding, On the Apparent shift of the rho meson mass in photoproduction, Phys. Lett. 19 (1966) 702–704. doi:10.1016/0031-9163(66)90451-3.
- [26] K. A. Olive, et al., Review of Particle Physics, Chin. Phys. C38 (2014) 090001. doi:10.1088/1674-1137/38/9/090001.
- [27] H. Alvensleben, et al., Precise determination of rho-omega interference parameters from photoproduction of vector mesons off nucleon and nuclei, Phys. Rev. Lett. 27 (1971) 888–892. doi:10.1103/PhysRevLett.27.888.
- [28] P. Langacker, Quark Mass Differences and $\rho - \omega$ Mixing, Phys. Rev. D20 (1979) 2983. doi:10.1103/PhysRevD.20.2983.
- [29] Y. Xu, O. Barannikova, H. Bichsel, X. Dong, P. Fachini, Y. Fisyyak, A. Kocoloski, B. Mohanty, P. Netrakanti, L. Ruan, M. C. Suarez, Z. Tang, G. van Buren, Z. Xu, Nuclear Instruments and Methods in Physics Research Section A: Accelerators, Spectrometers, Detectors and Associated Equipment 614 (1) (2010) 28 – 33. doi:http://dx.doi.org/10.1016/j.nima.2009.12.011, [link].
URL <http://www.sciencedirect.com/science/article/pii/S0168900209023067>
- [30] V. Rebyakova, M. Strikman, M. Zhalov, Coherent ρ and J/ψ photoproduction in ultraperipheral processes with electromagnetic dissociation of heavy ions at RHIC and LHC, Phys. Lett. B710 (2012) 647–653. arXiv:1109.0737, doi:10.1016/j.physletb.2012.03.041.
- [31] M. Drees, D. Zeppenfeld, Production of supersymmetric particles in elastic ep collisions, Phys. Rev. D 39 (1989) 2536–2546. doi:10.1103/PhysRevD.39.2536.
URL <http://link.aps.org/doi/10.1103/PhysRevD.39.2536>
- [32] M. Strikman, M. Tverskoy, M. Zhalov, Neutron tagging of quasielastic J/ψ photoproduction off nucleus in ultraperipheral heavy ion collisions at RHIC energies, Phys. Lett. B626 (2005) 72–79. arXiv:hep-ph/0505023, doi:10.1016/j.physletb.2005.08.083.
- [33] A. J. Baltz, M. J. Rhoades-Brown, J. Weneser, Heavy ion partial beam lifetimes due to Coulomb induced processes, Phys. Rev. E54 (1996) 4233–4239. doi:10.1103/PhysRevE.54.4233.
- [34] S. R. Klein, J. Nystrand, Interference in exclusive vector meson production in heavy ion collisions, Phys. Rev. Lett. 84 (2000) 2330–2333. arXiv:hep-ph/9909237, doi:10.1103/PhysRevLett.84.2330.
- [35] B. I. Abelev, et al., Observation of Two-source Interference in the Photo-production Reaction Au Au \rightarrow Au Au ρ^0 , Phys. Rev. Lett. 102 (2009) 112301. arXiv:0812.1063, doi:10.1103/PhysRevLett.102.112301.

- [36] T. Toll, T. Ullrich, The dipole model Monte Carlo generator Sartre 1, *Comput.Phys.Commun.* 185 (2014) 1835–1853. [arXiv:1307.8059](#), [doi:10.1016/j.cpc.2014.03.010](#).
- [37] Window Function.
URL https://en.wikipedia.org/wiki/Window_function
- [38] C. M. Tarbert, et al., Neutron skin of ^{208}Pb from Coherent Pion Photo-production, *Phys. Rev. Lett.* 112 (24) (2014) 242502. [arXiv:1311.0168](#), [doi:10.1103/PhysRevLett.112.242502](#).
- [39] A. Gardestig, C. J. Horowitz, G. A. Miller, Comment on "Neutron Skin of ^{208}Pb from Coherent Pion Photoproduction" [arXiv:1504.08347](#).
- [40] A. Accardi, et al., Electron Ion Collider: The Next QCD Frontier - Understanding the glue that binds us all [arXiv:1212.1701](#).
- [41] T. Toll, T. Ullrich, Exclusive diffractive processes in electron-ion collisions, *Phys.Rev.* C87 (2) (2013) 024913. [arXiv:1211.3048](#), [doi:10.1103/PhysRevC.87.024913](#).